Magnetic fluid based squeeze film in rough curved circular plates with Kozeny – Carman model based porous structure

R. M. Patel1*, G. M. Deheri2 and P. A. Vadher3[#3]

[#] 1. *Department of Mathematics, Gujarat Arts and Science College,*

 # 2 Department of Mathematics, Sardar Patel University, Vallabh Vidyanagar

 # 3 Department of Physics, Government Science College, Gandhinagar

#1 Gujarat University Gujarat

#2 S P university

#3 Gujarat University

rmpatel2711@gmail.com

gmdeheri@rediffmail.com

pragnavadher@rediffmail.com

Abstract**This investigation deals with the performance of Magnetic fluid based squeeze film in rough curved circular plates with various porous structures. The globular sphere model due to Kozeny – Carman and capillary fissures model of Irmay for porous structure have been subjected to investigations. The external magnetic field is considered to be oblique to the lower plate. Christenson and Tonder's model has been adopted to account for roughness. The associated statistically averaged generalized Reynolds' equation is solved for pressure distribution leading to the estimation of load carrying capacity. Results presented in graphical form show that the load carrying capacity increases with increasing values of magnetization parameter. Although, the effect of transverse roughness is in general, adverse there exists enough scope to minimize this adverse effect by the magnetic fluid lubrication at least in the case of Kozeny – Carman porous structure. Besides, the bearing records more load in the case of Kozeny – Carman porous structure as compared to the porous structure of Irmay**

Keywords**— Magnetic fluid, Squeeze film, Circular plates, Roughness, Porous structure**

I. INTRODUCTION

During the last decades the use of magnetic nano particles in the various engineering systems has attracted researchers all over the world. In fact, ferrofluids or magnetic fluids are stable colloidal suspension, consisting of ferromagnetic nano particles dispersed in a carrier liquid, while a surfactant is added to generate a coating layer preventing the flocculation of the particles. Ferrofluids experience body forces when an external magnetic field is applied and move through liquid imparting drag to it causing it flow. In addition, in magnetic gradient fields these fluids exhibit increased viscosity. Besides, ferrofluids undergo practically no ageing or separation. They remain liquid in a magnetic field and after removal of field recover their characteristics. Because of the above properties magnetic fluids are found to be useful in space ships which often travel in zero gravity regions. The advantage of magnetic fluid lubricant over the conventional ones is that the former can be retained at a desired location by an external magnetic field. Therefore, these fluids are used in sealed systems as in food preparation machines. In the area of medicine magnetic fluid based actuators are being developed for implanting artificial hearts which are driven by external magnetic fields. It is also well known that ferrofluid based viscous dampers are used in lens grading and robotics. [1 – 3]

The investigation carried out by Agrawal [4] regarding the effect of magnetic fluid on the performance of a porous inclined slider bearing indicated that the magnetization of the magnetic particles in the lubricant increased the load carrying capacity without changing the friction in the moving slider. Later on, Verma [5] dealt with the squeeze film behavior between porous plates and found that its performance with magnetic field was relatively better than conventional lubricants.

The squeeze film performance based on magnetic fluid lubrication in curved porous rotating circular plates was studied by Shah and Bhat [6]. It was shown that the curvature parameter significantly affected the bearing performance although; the magnetic strength was in force.

The magnetic fluid lubrication of a squeeze film between porous rotating circular plates was considered by Patel et. al. [7]. It was found that negative effect of porosity could be reduced by the positive effect of magnetization when variance negative occurred. The squeeze film performance in transversely rough annular plates under the presence of a magnetic fluid lubricant was discussed by Patel et. al. [8]. It was shown that the negatively skewed roughness turned in a relatively better performance. The performance of a magnetic fluid based squeeze film between transversely rough curved annular plates was improved by Deheri et. al. [9] by adopting a comparative study of the geometrical structures of the curved annular plates.

The analysis of squeeze film performance between curved annular plates with an electrically conducting fluid in the presence of a transverse magnetic field was presented by Lin et. al. [10]. According to the results obtained, the use of applied magnetic field registered an increase in the magneto hydrodynamic squeeze film pressure as compared to the case of non-conducting lubricant. The magnetic field effect characterized by the Hartmann number provided an enhancement to the load carrying capacity and response time especially for larger values of the curved shape parameter or the smaller values of the aspect ratio.

Here it has been sought to compare the effect of different porous structures on the performance of a ferrofluid based squeeze film in rough curved porous circular

ANALYSIS

The configuration of the bearing system is shown in Figure – I, which consists of two circular plates each of radius a. The upper plate has a porous facing of thickness l_1 which is backed by a solid wall. It moves normally towards an impermeable and flat lower plate with uniform velocity $\dot{h}_0 = \frac{dh_0}{dt}$.

The bearing surfaces are assumed to be transversely rough. Following the discussions of Christensen and Tonder [14 – 16] the geometry of the local film thickness can be thought of as consisting of two parts:

$$h(x) = \bar{h}(x) + h_s(x)$$

where $\bar{h}(x)$ is the mean film thickness and $h_s(x)$ is the deviation from the mean film thickness characterizing the random roughness of the bearing surfaces. $h_s(x)$ is considered to be stochastic in nature and governed by the probability density function $f(h_s)$, $-c \le h_s \le c$ where c is the maximum deviation from the mean film thickness. The mean α, the standard deviation σ and the parameter ε which is the measure of symmetry of random variable h_s, are governed by the relations

$$\alpha = E(h_s)$$
$$\sigma^2 = E[(h_s - \alpha)^2]$$

and

$$\varepsilon = E[(h_s - \alpha)^3]$$

where the expectancy operator E is defined by

$$E(R) = \int_{-c}^{c} R f(h_s) dh_s$$

while

$$f(h_s) = \begin{cases} \frac{35}{32c^7}(c^2 - h_s^2)^3, -c \le h_s \le c \\ 0, \text{elsewhere} \end{cases}$$

Assuming axially symmetric flow of the ferrofluid between the plates under an oblique magnetic field **H** = (H(r)cosϕ, 0, H(r)sinϕ) whose magnitude H vanishes at r = 0 and r = a, the modified Reynolds' equation governing the fluid film pressure p is [11 – 13]

$$\frac{1}{r}\frac{d}{dr}\left\{\left(h^3 + 3\sigma^2 h + 3h^2\alpha + 3h\alpha^2 + 3\sigma^2\alpha + \alpha^3 + \varepsilon + 12\psi l_1\right) r\frac{d}{dr}\left(p - 0.5\mu_0\bar{\mu}H^2\right)\right\} = 12\eta\dot{h}_0 \quad \ldots(1)$$

where $H^2 = Kr^2(a - r)/a$, $K = 10^{14} - 10^{16}$ A^2m^{-4} is chosen as to have a magnetic field of strength between the order 10^5 to 10^6. ψ is the permeability of the porous region, μ_0 is the permeability of the free space, $\bar{\mu}$ is the magnetic susceptibility and η is the fluid viscosity.

Because of the fact that the magnetic field comes out of a potential, the angle of inclination ϕ = ϕ(r, z) can be determined from

$$\cot\phi\frac{\partial\phi}{\partial r}+\frac{\partial\phi}{\partial z}=\frac{3r-2a}{2r(a-r)} \quad \ldots (2)$$

with the help of elliptic integrals depending on the value of a.

Case – I (a globular sphere model as shown in Figure – II). In this model the globular particles fill the porous material. The mean particle size is D_c.

In view of Kozney – Carman formulation [3] one finds that the permeability of the porous region takes the form

$$\psi=\frac{D_c^2e^3}{180(1-e)^2} \quad \ldots (3)$$

where e is the porosity.

Integrating the above equation (1) with respect to the boundary conditions

$$\frac{dp}{dr}=0 \text{ ,r = 0; p = 0, r = a} \quad \ldots (4)$$

one gets the expression for pressure distribution as

$$p=0.5\mu_0\bar{\mu}H^2+\frac{3\eta\dot{h}_0}{h^3+3\sigma^2h+3h^2\alpha+3h\alpha^2+3\sigma^2\alpha+\alpha^3+\varepsilon+12\psi l_1}\left(r^2-a^2\right) \quad \ldots (5)$$

Introducing the non dimensional quantities

$$P=-\frac{ph_0^3}{\eta a^2\dot{h}_0} \qquad \mu^*=-\frac{\mu_0\bar{\mu}h_0^3}{\eta\dot{h}_0} \qquad R=\frac{r}{a}$$

$$\bar{\psi}=\frac{D_c^2l_1}{h_0^3} \qquad \bar{h}=\frac{h}{h_0} \qquad \bar{h}1=\frac{h_1}{h_0}$$

$$\bar{h}2=\frac{h_2}{h_0} \qquad \sigma^*=\frac{\sigma}{h_0} \qquad \alpha^*=\frac{\alpha}{h_0} \qquad \varepsilon^*=\frac{\varepsilon}{h_0^3}$$

and

$$g(\bar{h}) = 1 + 3\sigma^{*2} + 3\alpha^* + 3\alpha^{*2} + 3\sigma^{*2}\alpha^* + \alpha^{*3} + \varepsilon^* \quad \ldots (6)$$

the nondimensional pressure can be had from

$$P=\frac{\mu^*}{2}R^2(1-R)+\frac{3(1-R^2)}{g(\bar{h})+\frac{\bar{\psi}\,e^3}{15(1-e)^2}} \quad \ldots (7)$$

The load carrying capacity of the bearing in non-dimensional form can be expressed as

$$W=\frac{\mu^*}{40}+\frac{3}{4}\left[\frac{1}{g(\bar{h})+\frac{\bar{\psi}e^3}{15(1-e)^2}}\right] \quad \ldots (8)$$

The response time $\Delta\bar{t}$ taken by the upper plate to reach a film thickness h_2 from an initial film thickness h_1 can be determined in dimensionless form as

$$\Delta\bar{t} = -W \int_{\bar{h}_1}^{\bar{h}_2} \frac{d\bar{h}}{\bar{h}^3 + 3\sigma^{*2}\bar{h} + 3\bar{h}^2\alpha^* + 3\bar{h}\alpha^{*2} + 3\sigma^{*2}\alpha^* + \alpha^{*3} + \varepsilon^* + 12\bar{\psi}} \quad \ldots (9)$$

where

$$\bar{h}_1 = \frac{h_1}{h_0},\ \bar{h}_2 = \frac{h_2}{h_0} \text{ and } \bar{h} = \frac{h}{h_0}$$

Case – II (a capillary fisher's model as shown in figure – III). This model comprises of three sets of mutually orthogonal fishers (mean solid size D_s). No loss of hydraulic gradient at the junctions was assumed by Irmay [17] who obtained the expression for the permeability as

$$\psi = \frac{\left(1 - m^{2/3}\right) D_s^2}{12m} \quad \ldots (10)$$

where m = 1 – e, e being the porosity.

Solving equation (1) under the boundary conditions (4), in view of the dimensionless quantities (6) the expression for non-dimensional pressure distribution is found to be

$$P = \frac{\mu^*}{2} R^2 (1 - R) + \frac{3(1 - R^2)}{g(\bar{h}) + \frac{\bar{\psi}(1 - m^{2/3})}{m}} \quad \ldots (11)$$

where

$$\bar{\psi} = \frac{D_s^2 l_1}{h_0^3} \quad \ldots (12)$$

Then the governing expression for nondimensional form of load carrying capacity of the bearing is derived as

$$W = \frac{\mu^*}{40} + \frac{3}{4}\left[\frac{1}{g(\bar{h}) + \frac{\bar{\psi}(1 - m^{2/3})}{m}}\right] \quad \ldots (13)$$

Lastly, the response time $\Delta\bar{t}$ taken by the upper plate to reach a film thickness h_2 from an initial film thickness h_1 can be determined in dimensionless form as

$$\Delta\bar{t} = -W \int_{\bar{h}_1}^{\bar{h}_2} \frac{d\bar{h}}{\bar{h}^3 + 3\sigma^{*2}\bar{h} + 3\bar{h}^2\alpha^* + 3\bar{h}\alpha^{*2} + 3\sigma^{*2}\alpha^* + \alpha^{*3} + \varepsilon^* + 12\bar{\psi}} \quad \ldots (14)$$

where

$$\bar{h}_1 = \frac{h_1}{h_0},\ \bar{h}_2 = \frac{h_2}{h_0} \text{ and } \bar{h} = \frac{h}{h_0}$$

RESULTS AND DISCUSSIONS

It is seen from Equations 7 and 11 that the non-dimensional pressure increases by while the enhancement in dimensionless load carrying capacity is as indicated by equations 8 and 13 due to magnetization, as compared to the case of traditional lubricant. At least the load carrying capacity increases by 1.3 % owing to magnetic fluid lubrication. Probably, this may be due to the fact that the effective viscosity of the lubricant gets increased due to magnetization resulting in increased pressure. In the case of bearings with smooth surfaces this study reduces to the effect of various porous structures on the performance of a magnetic fluid based squeeze film. Further, setting the magnetization parameter to be zero, one obtains the effect of various porous structures on the circular squeeze film.

Figures (1–15) deal with the variation of load carrying capacity with respect to various parameters for globular sphere model of Kozeny Carman, while the distribution of load carrying capacity with respect to the capillary fisher's model of Irmay is presented in Figures (16–30). It can be observed from equations 8 and 13 that the expression is linear with respect to the magnetization parameter □*. Accordingly, it would lead to increased load carrying capacity as can be seen from Figures (1–5) and (16–20), It is easily observed that the load carrying capacity increases significantly in the case of Kozeny Carman model as compared to Irmay's model. Further the effect of porosity and skewness on the distribution of load carrying capacity with respect to □* is almost negligible in the case of globular sphere model.

The effect of standard deviation on the variation of load carrying capacity with respect to Kozeny Carman model is given in Figures (6–9) while Figures (21–24) show the profile of load carrying capacity with respect to the standard deviation in the case of Irmay's model. It is noticed that the increase in the values of standard deviation causes decreased load carrying capacity as a result of which the standard deviation introduces an adverse effect on the squeeze film performance. Figures (8), (9) make it clear that in the case of Kozeny Carman model the effect of porosity and skewness on the distribution of load carrying capacity with respect of standard deviation is negligible, while Figure (24) informs that the effect of skewness on the load profile with respect to the standard deviation is not that significant.

The effect of variance on the distribution of load carrying capacity with respect to Kozeny Carman model and Irmay's model are supplied in Figures (10–12) and Figures (25–27) respectively. It is observed that the positive variance decreases the load carrying capacity for both the models while the load carrying capacity gets increased due to variance (–ve). It is interesting to find that the effect of porosity and skewness on the distribution of load carrying capacity with respect to variance is almost negligible for both the models. The effect of skewness presented in Figures 13, 14, 28 and 29 ensures that the trends of load carrying capacity with respect to skewness are alike to that of variance. Therefore, the combined effect of negatively skewed roughness and variance (–ve) is significantly positive. In addition, for the Kozeny Carman model the combined effect of □ and e on the distribution of load carrying capacity with respect to skewness is negligible while the effect of e on the variation of load carrying capacity with respect to skewness is not that significant in the case of Irmay's model. Lastly, the combined effect of □ and e is considerably adverse as can be seen from Figures 15 and 30.

A close look at the figures reveals that the negative effect of porosity can be minimized to a large extent by the positive effect of magnetization in the case of negatively skewed roughness with regards to globular sphere model. However, it is manifest that the variance plays a central role for a relatively better performance in the case of Irmay's model.

II. CONCLUSION

This study indicates that the Kozeny Carman model may be more suitable for this type of bearing systems. The roughness must be given due consideration while designing the bearing system even if suitable magnetic strength is in force. Lastly, the bearing system supports certain amount of load in the absence of flow for both the models which is very unlikely in the case of conventional lubricants.

REFERENCES

[1] Rosenweig, R. E., Ferrohydrodynamics, Cambridge University Press, New York (1985).

[2] Zahn, M., Rosenweigh, R. E., Stability of magnetic fluid penetrating through a porous medium with uniform magnetic field oblique to the surface, *IEEE Transactions of Magnetics*, 16, (1980).

[3] Jun Liu, Analysis of a porous elastic sheet damper with a magnetic fluid, *Journal of Tribology*, 131, 0218011-15, 2009.

[4] Agrawal, V. K., Magnetic fluid based porous inclined slider bearing, Wear, 107, 133-139, 1986.

[5] Verma, P. D. S., Magnetic fluid based squeeze films, *International Journal of Engineering Sciences*, 24(3), 395-401, 1986.

[6] Shah, R. C., Bhat, M. V., Squeeze film based on magnetic fluid in curved porous rotating circular plates, *Journal of Magnetism and Magnetic Materials*, 208, 115-119, 2000.

[7] Patel, H., Deheri, G. M. and Patel, R. M., A study of magnetic fluid based squeeze film between porous rough elliptical plates, *Journal of Modeling Design and Management of Engineering Systems*, 41, 11-20, 2009.

[8] Patel, R. M., Deheri, G. M. and Vadher, P. A., Magnetic fluid based squeeze film between annular plates and transverse surface roughness effect, Journal of Engineering, Annals of Faculty of Engineering, *Hunedoara*, 8(1), p.p. 51-56, 2010.

[9] Deheri, G. M., Patel, R. M. and Abhangi, D., Magnetic fluid based squeeze film between transversely rough curved annular plates: a comparative study, *Industrial Lubrication and Tribology*, 63(4), 254-270, 2011.

[10] Jaw-Ren Lin, Rong-Fang Lu, Won-Hsion Liao, Analysis of magneto-hydrodynamic squeeze film characteristics between curved annular plates, *Industrial Lubrication and Tribology*, 56(5), 300-305, 2004.

[11] Bhat, M. V., Deheri, G. M., Magnetic fluid based squeeze film in curved porous circular disks, *Journal of Magnetism and Magnetic Material*, 127, 159-162, 1993.

[12] Patel, R. M., Deheri, G. M., On the behavior of squeeze film formed by a magnetic fluid between curved annular plates, *Indian Journal of Mathematics*, 44, 353-359, 2002.
[13] Patel, R. M., Deheri, G.., Magnetic fluid based squeeze film behavior between annular plates and surface roughness effect, *Proceedings of AIMETA International Tribology Conference*, 631-638, 2004.
[14] Christensen, H., Tonder, K., Tribology of rough surfaces, *Stochastic models of hydrodynamic lubrication, SINTEF, Section for Machine Dynamics in Tribology, Technical University of Norway, Trondheinm, Norway*, Report No.10/69-18, 1969a.
[15] Christensen, H., Tonder, K., Tribology of rough surfaces, parametric study and comparison of lubrication models, *SINTEF, Section for Machine Dynamics in Tribology, Technical University of Norway, Trondheinm, Norway, Report No.22/69-18, 1969b.*
[16] Christensen, H., Tonder, K., The hydrodynamic lubrication of rough bearing surfaces of finite width, *ASME-ASLE Lubrication conference Cincinnati, Ohio, October 12-15, Lub-7, 1970.*
[17] Irmay, S., Flow of liquid through cracked media, *Bulletin of Research Council*, Isr., 5 A(1), 84, 1955.

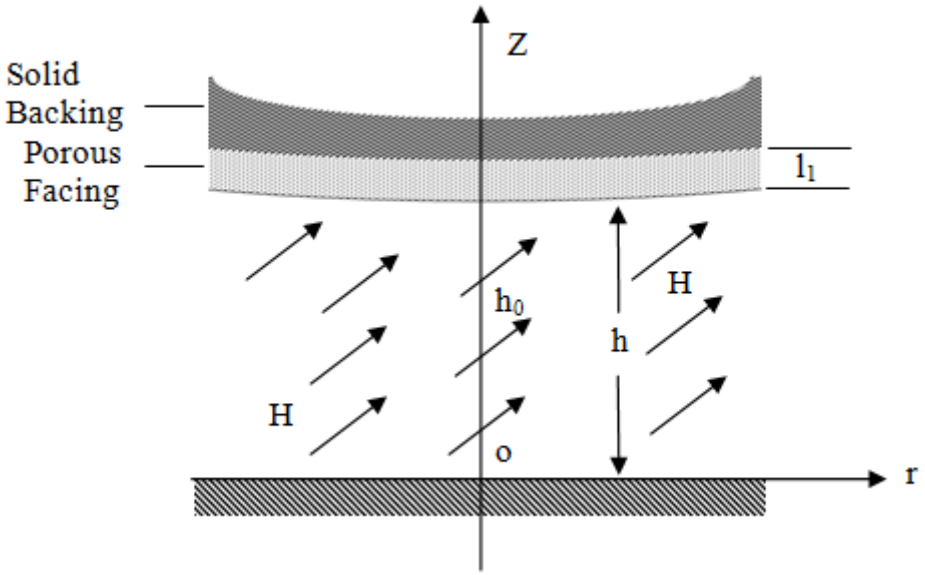

Figure – I Configuration of the bearing system

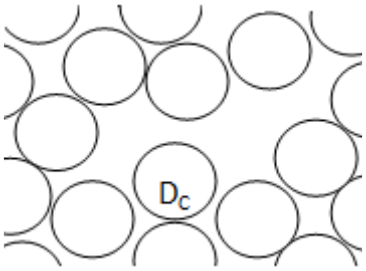

Figure – II Structure model of porous sheets given by Kozeny – Carman

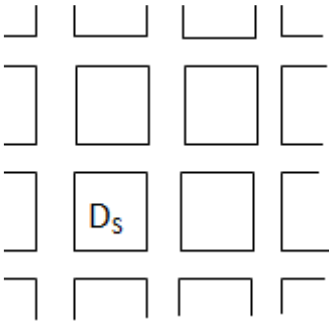

Figure – III Structure model of porous sheets given by Irmay

Figure: 1 Variation of load carrying capacity with respect to μ* and σ*.

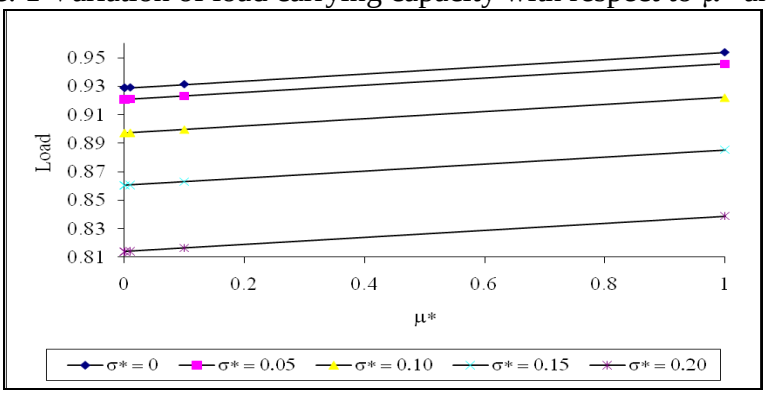

Figure: 2 Variation of load carrying capacity with respect to μ* and α*.

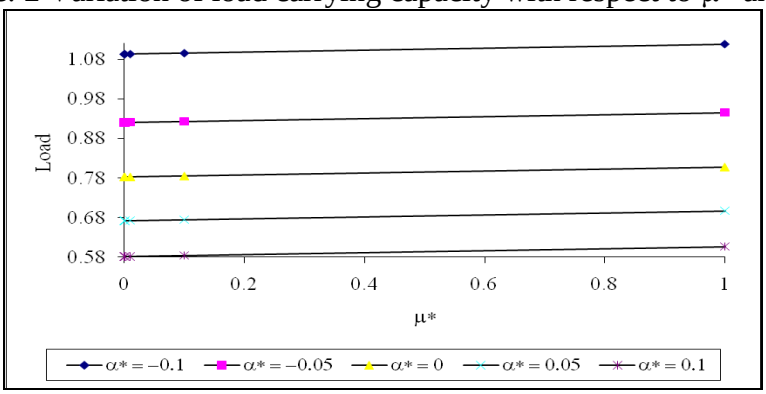

Figure: 3 Variation of load carrying capacity with respect to μ* and ε*.

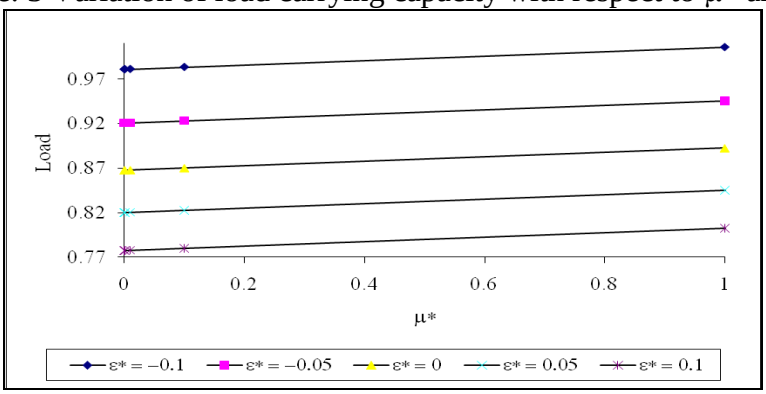

Figure: 4 Variation of load carrying capacity with respect to μ* and ψ.

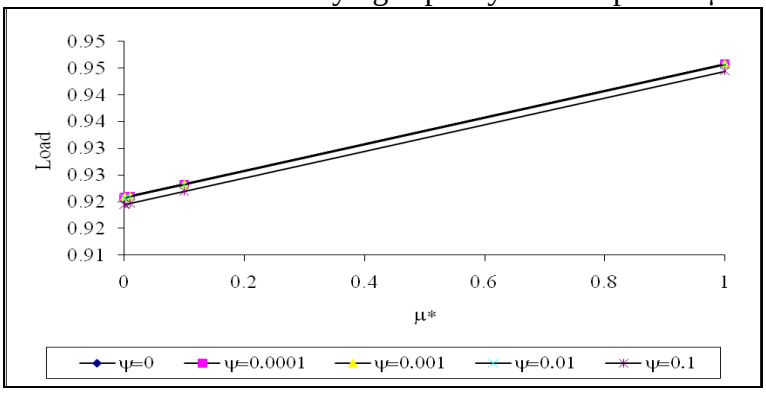

Figure: 5 Variation of load carrying capacity with respect to μ* and e.

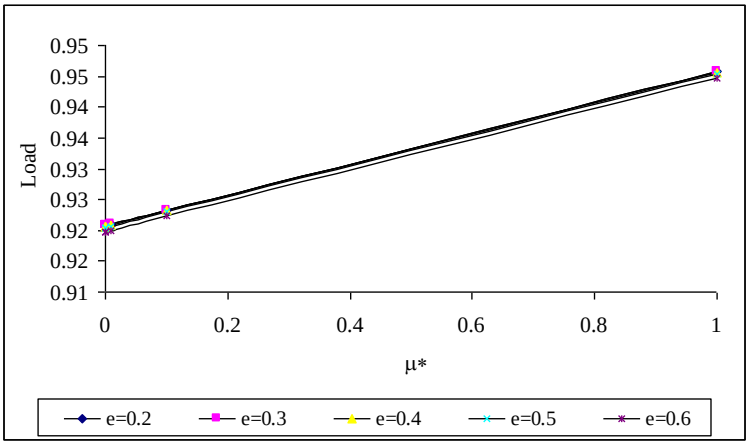

Figure: 6 Variation of load carrying capacity with respect to σ* and α*.

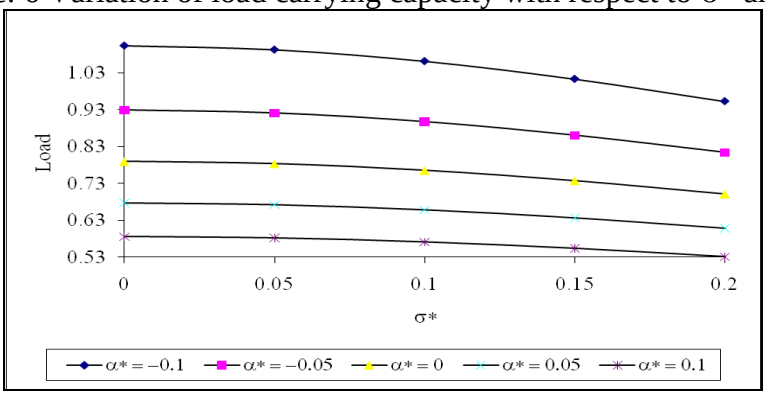

Figure: 7 Variation of load carrying capacity with respect to σ* and ε*.

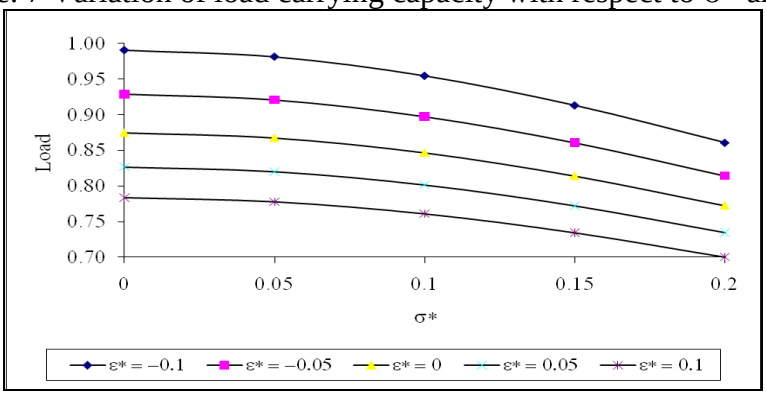

Figure: 8 Variation of load carrying capacity with respect to σ* and ψ.

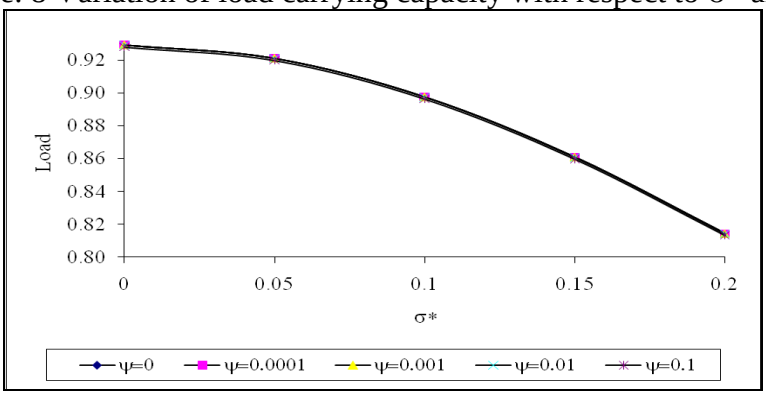

Figure: 9 Variation of load carrying capacity with respect to σ* and e.

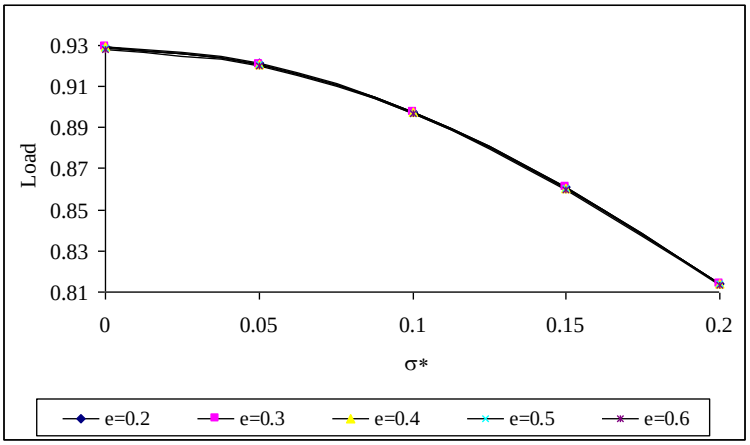

Figure: 10 Variation of load carrying capacity with respect to α* and ε*.

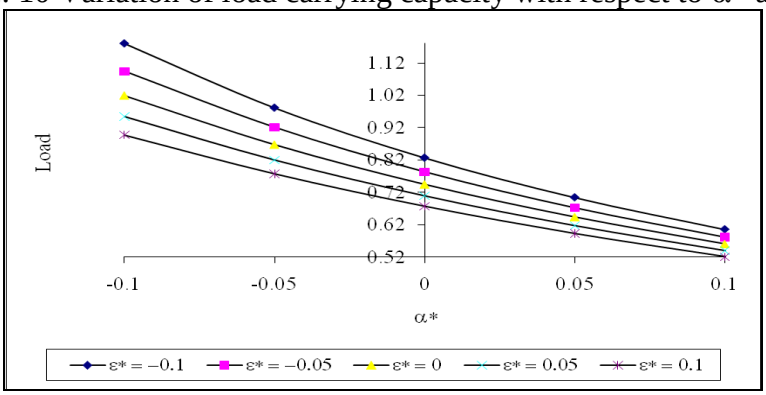

Figure: 11 Variation of load carrying capacity with respect to α* and ψ.

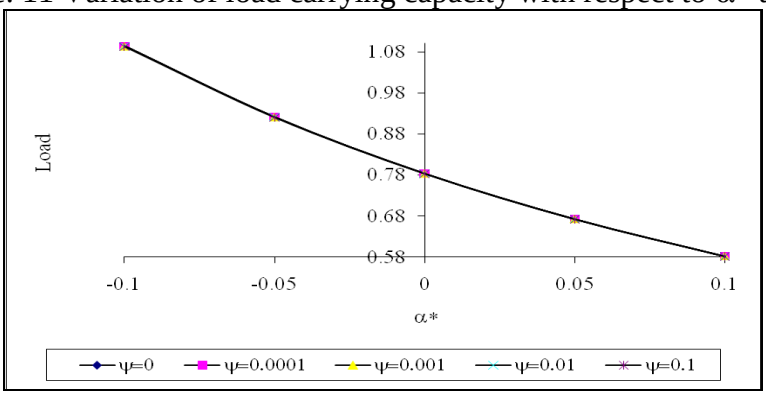

Figure: 12 Variation of load carrying capacity with respect to α* and e.

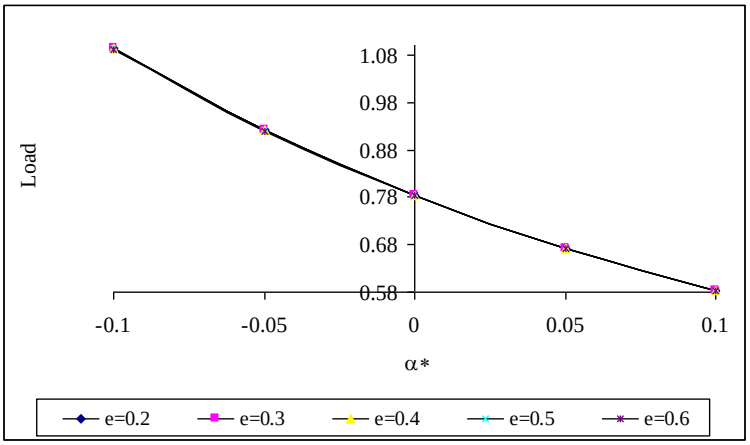

Figure: 13 Variation of load carrying capacity with respect to ε* and ψ.

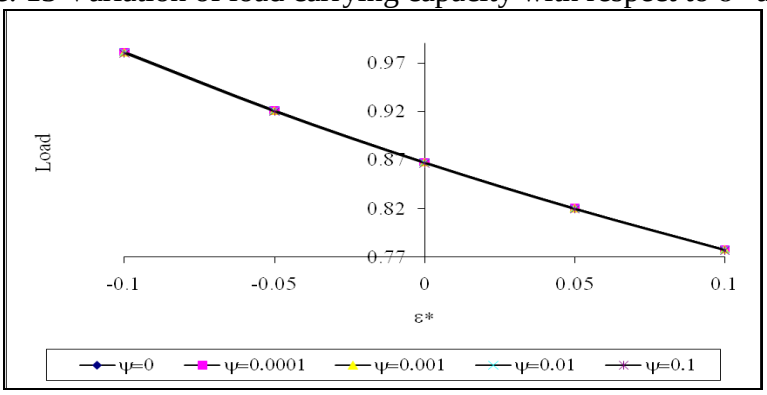

Figure: 14 Variation of load carrying capacity with respect to ε* and e.

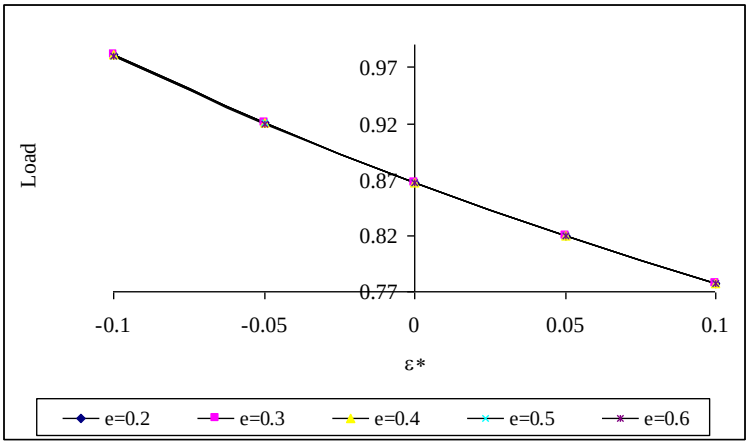

Figure: 15 Variation of load carrying capacity with respect to ψ and e.

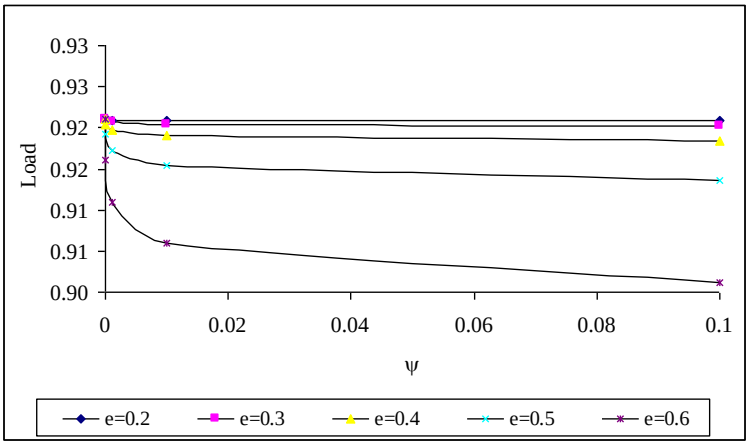

Figure: 16 Variation of load carrying capacity with respect to μ* and σ*.

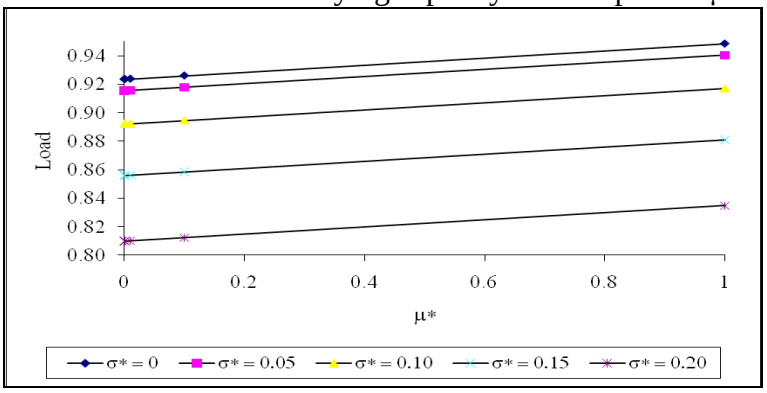

Figure: 17 Variation of load carrying capacity with respect to μ* and α*.

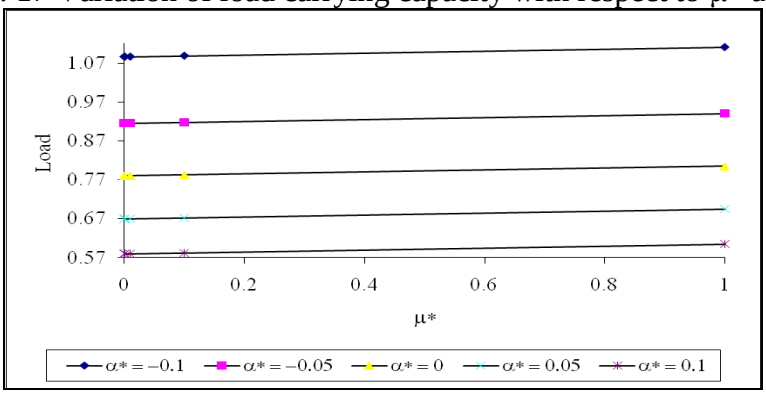

Figure: 18 Variation of load carrying capacity with respect to μ* and ε*.

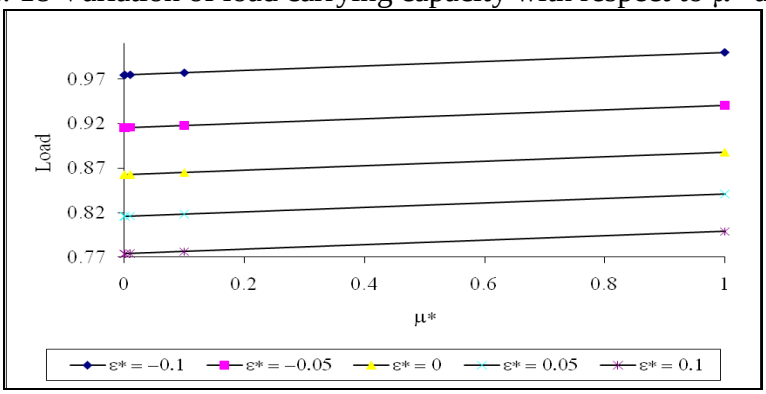

Figure: 19 Variation of load carrying capacity with respect to μ* and ψ.

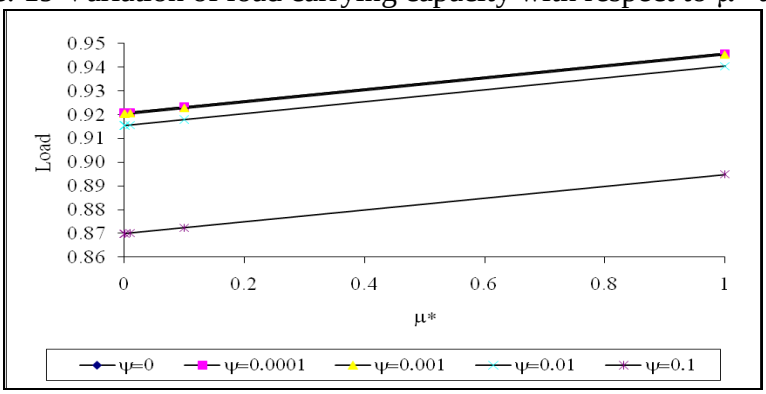

Figure: 20 Variation of load carrying capacity with respect to μ* and e.

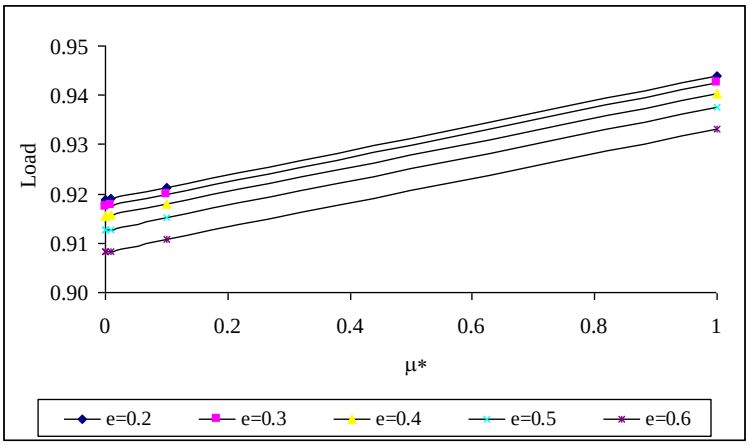

Figure: 21 Variation of load carrying capacity with respect to σ* and α*.

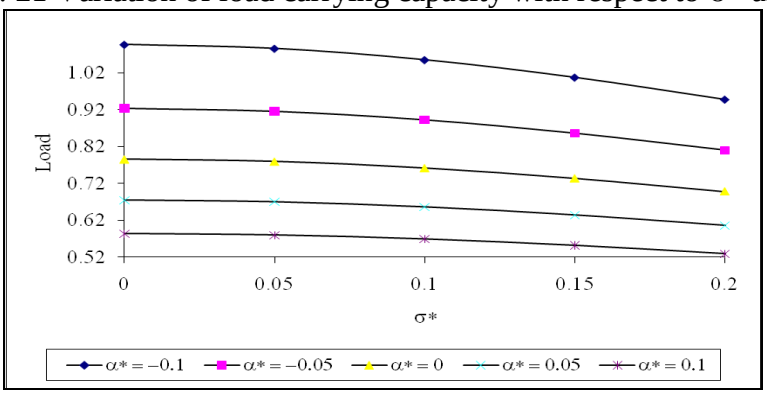

Figure: 22 Variation of load carrying capacity with respect to σ* and ε*.

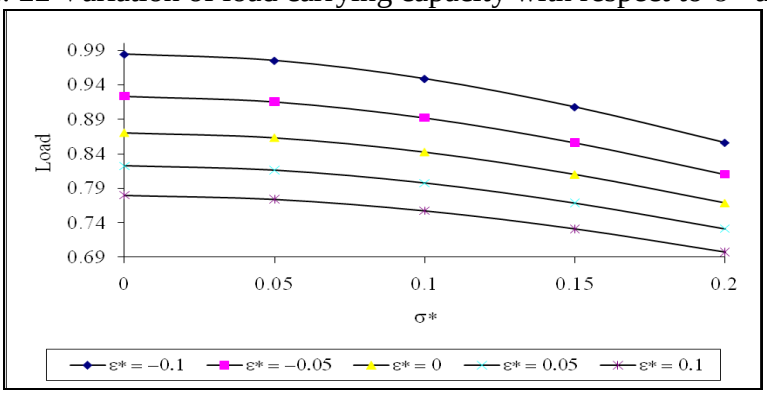

Figure: 23 Variation of load carrying capacity with respect to σ* and ψ.

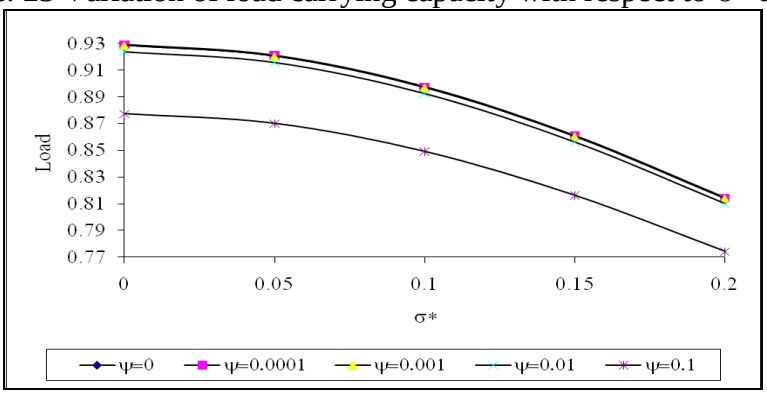

Figure: 24 Variation of load carrying capacity with respect to σ* and e.

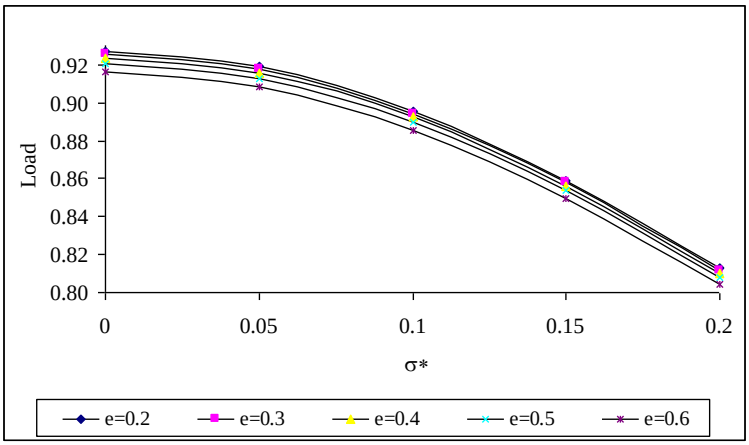

Figure: 25 Variation of load carrying capacity with respect to α∗ and ε∗.

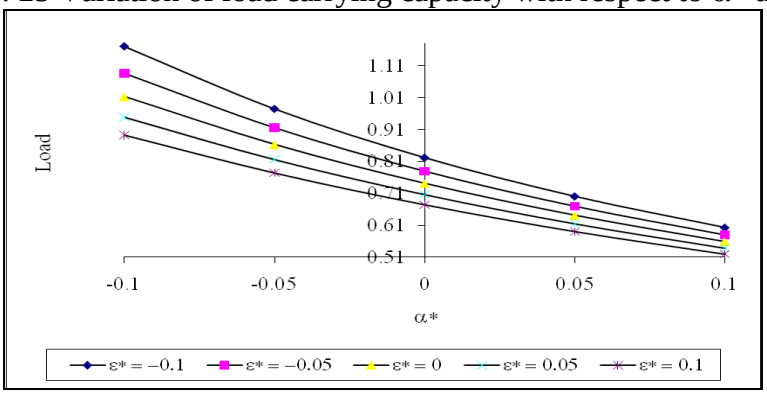

Figure: 26 Variation of load carrying capacity with respect to α∗ and ψ.

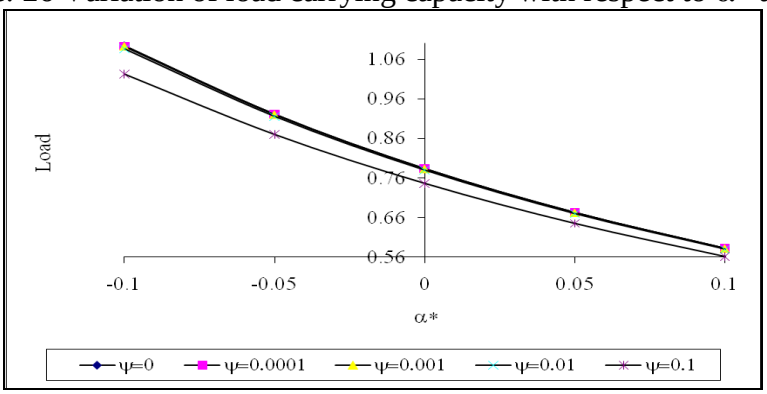

Figure: 27 Variation of load carrying capacity with respect to α∗ and e.

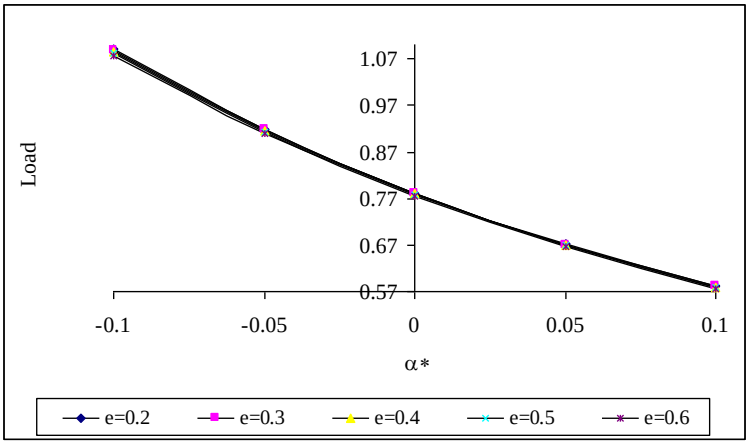

Figure: 28 Variation of load carrying capacity with respect to ε∗ and ψ.

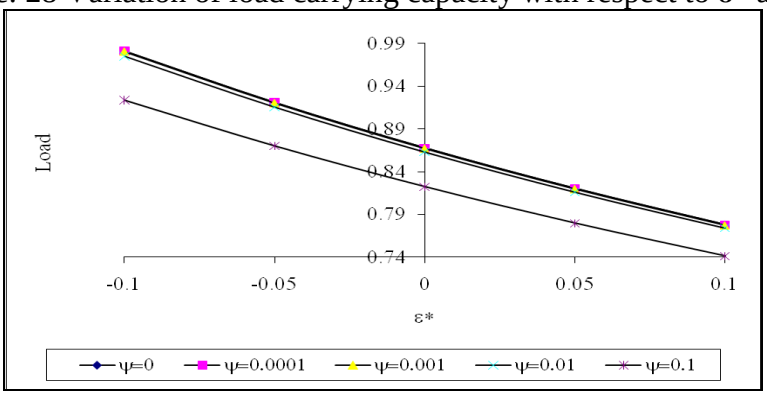

Figure: 29 Variation of load carrying capacity with respect to ε* and e.

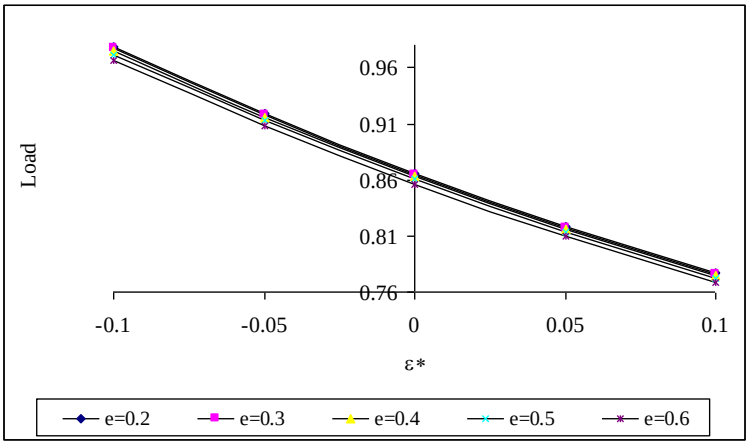

Figure: 30 Variation of load carrying capacity with respect to ψ and e.